Title: **Erasable Hippocampal Neural Signatures Predict Memory Discrimination**

Authors: Kinsky, Nathaniel R.,[1,3,5,6] Orlin, Daniel O,[3,4,5] Ruesch, Evan A.[3], Diba, Kamran[1,2], Ramirez, Steve[3,6]

1 – Department of Anesthesiology, University of Michigan Medical School, Ann Arbor, MI 48109

2 – Neuroscience Graduate Program, University of Michigan, Ann Arbor, MI 48109

3 – Center for Systems Neuroscience, Boston University, Boston, MA 02451

4 – Neuroscience Graduate Program, Oregon Health & Science University, Portland, OR 97239

5 – These authors contributed equally to this work

6 – Corresponding authors. Correspondence should be addressed to N.R.K (nkinsky@umich.edu) or S.R. (dvsteve@bu.edu)

Abstract: We leveraged the spatial-temporal resolution of in vivo calcium imaging in freely moving mice to interrogate how blocking contextual fear memory consolidation impacted learning-related hippocampal dynamics. We found that memory specificity correlated with the amount of cell turnover between a shock and neutral arena and that learning caused context-specific remapping. Blocking protein synthesis following learning promoted an acute suppression of neural activity, arrested learning-related remapping, and induced amnesia. Lastly, freeze-predicting neural ensembles emerged following learning, and their coordinated activity required protein synthesis. We conclude that context-specific place field remapping and the development of coordinated ensemble activity support contextual fear memory consolidation and require protein synthesis.

Main Text:

The consolidation of newly formed memories requires protein synthesis (Barondes & Cohen, 1967; Ryan et al., 2015; Squire & Barondes, 1973). Protein synthesis is necessary to sustain learning-related structural and functional changes in hippocampus (HPC) neurons (Frey & Morris, 1998) and maintain the spatial firing fields (place fields) of HPC neurons formed in novel environments (Agnihotri et al., 2004). Contextual fear conditioning (CFC) has been reported to induce a robust context-specific reorganization (i.e. remapping) of HPC place fields that subsequently stabilize (Moita et al., 2004; Wang et al., 2012), supporting the idea that associative learning causes remapping of the HPC spatial code and that the maintenance of this code requires new protein synthesis. However, despite the relationship between stable HPC spatial activity and long term memory, little is known about how blocking consolidation impacts remapping and stability of previously acquired HPC spatial representations. To that end, we combined *in vivo* calcium imaging with CFC and systemic administration of the protein synthesis inhibitor, anisomycin, to track the evolution, remapping, and stabilization of HPC place fields under healthy and amnestic conditions. We further explored how between-animal variability in HPC dynamics influenced memory specificity and how blocking protein-synthesis impacted the development of HPC ensembles active during freezing behavior.

Following two days (day -2 and -1) of pre-exposure to an operant chamber (shock arena) and open-field (neutral arena) mice received a mild foot-shock on day 0 (training), after which they were moved to their home cage and immediately given systemic injections of anisomycin (ANI group) or vehicle (CTRL group). We then performed a short-term memory test 4 hours after

shock and three tests of long-term memory recall 1, 2, and 7 days after shock (Figure 1A) by measuring freezing behavior. We titrated the shock level during training such that the mice froze significantly more in the shock arena relative to the neutral arena following learning while still exploring the majority of both arenas. We observed a range of freezing levels during the day 1 and 2 memory tests (Figure S1A) and divided Control mice into two groups: Learners, who froze significantly more in the shock arena, and Non-Learners, who either generalized freezing or froze at low levels in both arenas (Figures 1B, 1G, Figure S1B). In contrast, mice in the ANI group exhibited no difference in freezing between arenas at any time point, suggesting that anisomycin impaired a context-specific fear memory (Figure 1C). Both the control and ANI groups exhibited significant increases in freezing in the shock arena during the 4 hour test (Figure 1D, Figure S1A), though the ANI group behavior could be by either contextual fear or non-specific effects of anisomycin (Figure S2) since they froze at high levels in both arenas.

Prior to training, we virally expressed the genetically encoded calcium indicator GCaMP6f (Chen et al., 2013) in pyramidal neurons in region CA1 of the dorsal hippocampus (Figure 1C) of our mice and visualized their activity using a miniaturized epifluorescence microscope (Figure 1F, Ghosh et al., 2011; Ziv et al., 2013). We identified a large number of neurons in each 10 minute session (n = 128 to 1216), extracted their corresponding calcium traces and tracked them between sessions throughout the CFC task, which allowed us to determine the long-term evolution of the HPC neural code (Figure 1C,F).

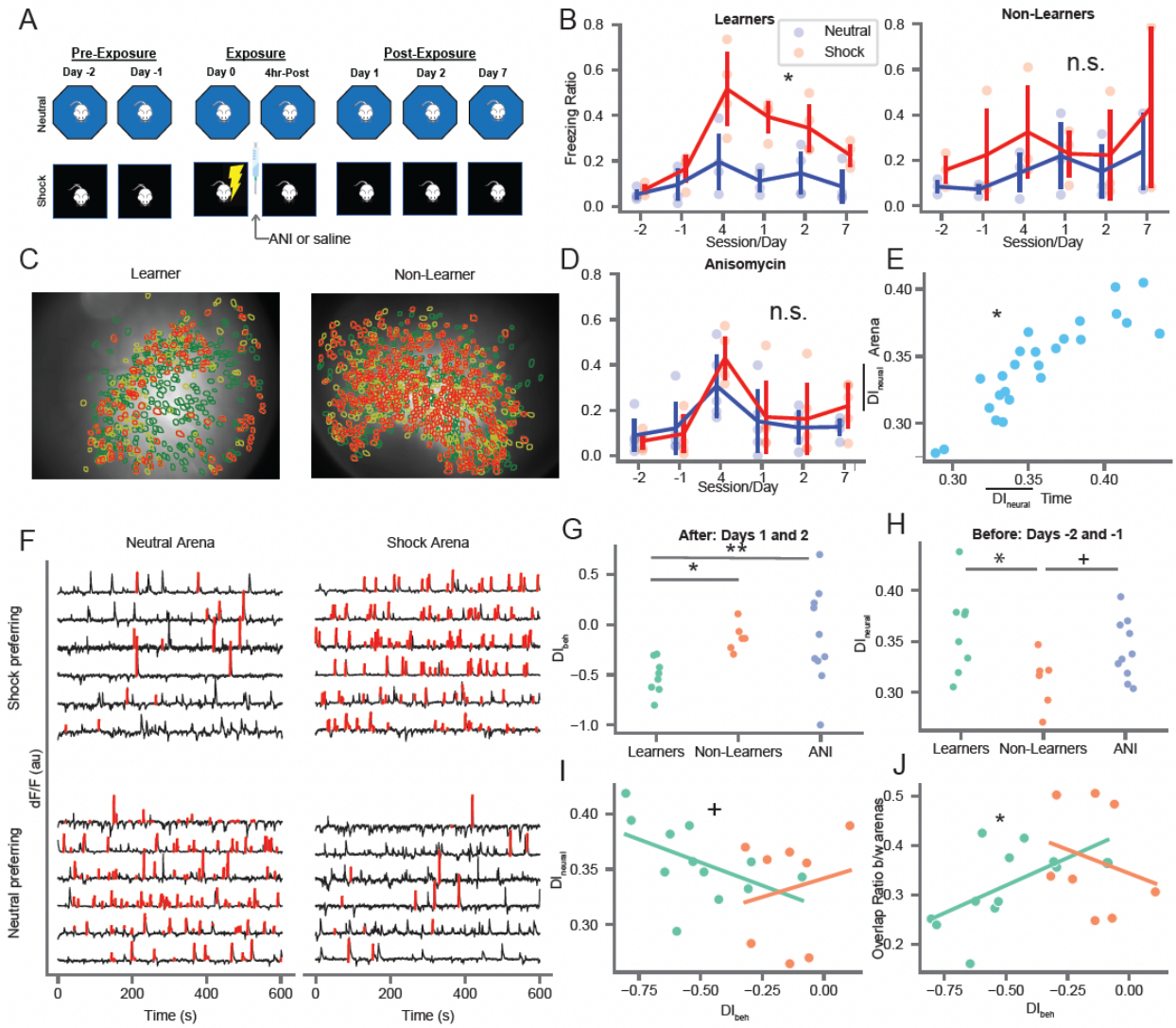

Figure 1: Neural discrimination between arenas predicts specificity of fear learning. A) Schematic of the behavioral paradigm. Mice freely explored two distinct arenas (neutral and shock) for 10 minutes each day. Mice underwent mild contextual fear conditioning on day 0 in the shock arena followed by immediate I.P. administration of anisomycin or vehicle in their home cage. Memory recall test were conducted 4 hours post-shock and 1, 2, and 7 days post-shock. The time of each session is referenced to the shock session. **B)** (left) Learner (Control) mice freezing on all days. Red = shock arena, Blue = neutral arena. *p=1.3e-0.5 shock – neutral freezing from days -2/-1 to days 1/2 one-sided t-test (n=4 mice). (right) Same but for Non-Learner (Control) mice (n=3 mice). **C)** (left) Neural overlap plots between Neutral and Shock arenas for an example Learner mouse on day -1, before shock. Green = cells active in the Shock arena only, yellow = cells active in the Neutral arena only, orange = cells active in both arenas. (right) Same for example Non-Learner on day -2 showing higher overlap of active cells between arenas. **D)** Same as B but for ANI group **E)** Mean neural discrimination between arenas (same day, days -2 to -1 and 1 to 2) vs. within arenas (same arena, days -2 and -1, days 1 and 2). *p=2.35e-8 (⊠ =-0.56) Spearman correlation. **F)** Example calcium activity from the Learner mouse shown in C (left) for cells active in both arenas. Black = calcium trace, Red = putative spiking activity during transient rises. Top row shows Shock arena preferring cells, bottom row shows Neutral arena preferring cells. **G)** Behavioral discrimination between arenas after shock (Days 1-2) shows formation of a specific fear memory for Learners only, by definition (positive = more freezing in neutral arena, negative = more freezing in shock arena, 0 = equal freezing in both arenas). *p=0.022, **p=0.00038 1-sided t-test **H)** Neural discrimination between arenas BEFORE shock indicates Learners formed more distinct representations of each arena prior to learning. Same conventions as F. *p=0.030, +p=0.059 two-sided t-test. **I)** Neural overlap between arenas correlates with specificity of fear memory on days 1-2 for Learners but not Non-Learners. +p=0.059 (rho=-0.56) for Learners. **J)** Same as I) but plotting behavioral discrimination vs. overlap ratio between arenas on Days 1-2. *p=0.033 (rho=0.61).

Previous work has demonstrated that higher overlap between HP neurons active in two distinct arenas correlates with increased generalization of a contextual fear memory (Cai et al., 2016). Accordingly, we hypothesized that the distinctiveness of the HPC neural code between arenas would predict how much mice froze in the neutral arena. We calculated a behavioral

discrimination index (DI_{frz}) to quantify how much each animal froze in the shock vs. neutral arena. Positive DI values indicated higher freezing in the shock compared to neutral arena. By definition, Learners exhibited higher DI_{frz} levels than Non-Learners on days 1 and 2; Learner DI_{frz} levels were also higher than mice in the ANI group (Figure 1G). We noticed that many neurons exhibited strong changes in mean event rate between arenas (Figure 1F) and calculated a neural discrimination index (DI_{neural}) to quantify the distinctiveness of neural activity between arenas (0 = similar, 1 = distinct). Same-day neural discrimination between arenas correlated strongly with across-day neural discrimination in the same arena (Figure 1E, Figure S1C). This indicates that mice exhibit natural variability in neural discrimination which is invariant between different arenas and across time. Interestingly, we noticed that DI_{neural} was significantly higher for Learners than Non-Learners in the sessions *prior to* the shock (Figure 1H). This inherent variability influences which neurons are active in different arenas and predisposes mice with higher neural discrimination to form context-specific fear memories.

We next utilized a regression analysis to determine if neural discrimination during memory recall *after* shock likewise correlated with memory discrimination. We utilized two metrics to quantify the distinctiveness of the HPC neural code between arenas: 1) the aforementioned DI_{neural} metric, which is based on cells that are active in both arenas, and 2) the overlap ratio of neurons active in both arenas divided by the total number of cells active in either arena, in order to account for cells that are silent in one arena. We found that overlap ratio was significantly correlated with DI_{frz} for Learners, but not for Non-Learners, on days 1-2 (Figure 1J); likewise, the correlation between DI_{frz} and DI_{neural} approached significance for Learners but not for Non-Learners on days 1-2 (Cai et al., 2016; Figure 1I). Together, our results suggest that mice which segregate experiences in their HPC neural code were more capable of forming discrete long-term memories and that the distinctiveness in HPC activity predicts the specificity of a CFC memory.

Next, we probed how arresting protein synthesis impacted HPC dynamics. We hypothesized that, by preventing plasticity, ANI administration would slow or stop the normal rate of cell turnover observed in Control mice (Figure 2A). Surprisingly, we found that ANI administration rapidly accelerated cell turnover, indicated by lower overlap of active cells between sessionsm from the day 0 session to the 4 hour session when compared to Control mice (Figure 2A-C). This effect was driven by a sharp decrease in the number of active neurons recorded in the ANI group at the 4 hour session, despite the ANI group having comparable freezing levels to Control mice at this time point (Figure 1D, Figure S1A). This acute acceleration was followed by a decrease in cell turnover rate from the 4 hour to day 1 session for ANI compared to Control mice (Figure 2B-C). We observed no difference in the mean height of calcium transients for all neurons active before, during, and after ANI administration, indicating that the observed decrease in number of active neurons is not due to depletion of the GCaMP protein (Figure S4E-F). This decrease in activity was not due to a global suppression of theta activity reported for intracranial infusions of protein synthesis inhibitors (Barondes & Cohen, 1966; Sharma et al., 2012), since we observed preserved theta activity, theta modulation of spiking, and sharp wave ripple activity in the ~5 hours following anisomycin administration in a rat recording (Figure S7). This indicates that blocking protein synthesis following learning reduces activity in a subset of neurons, presumably those involved in learning.

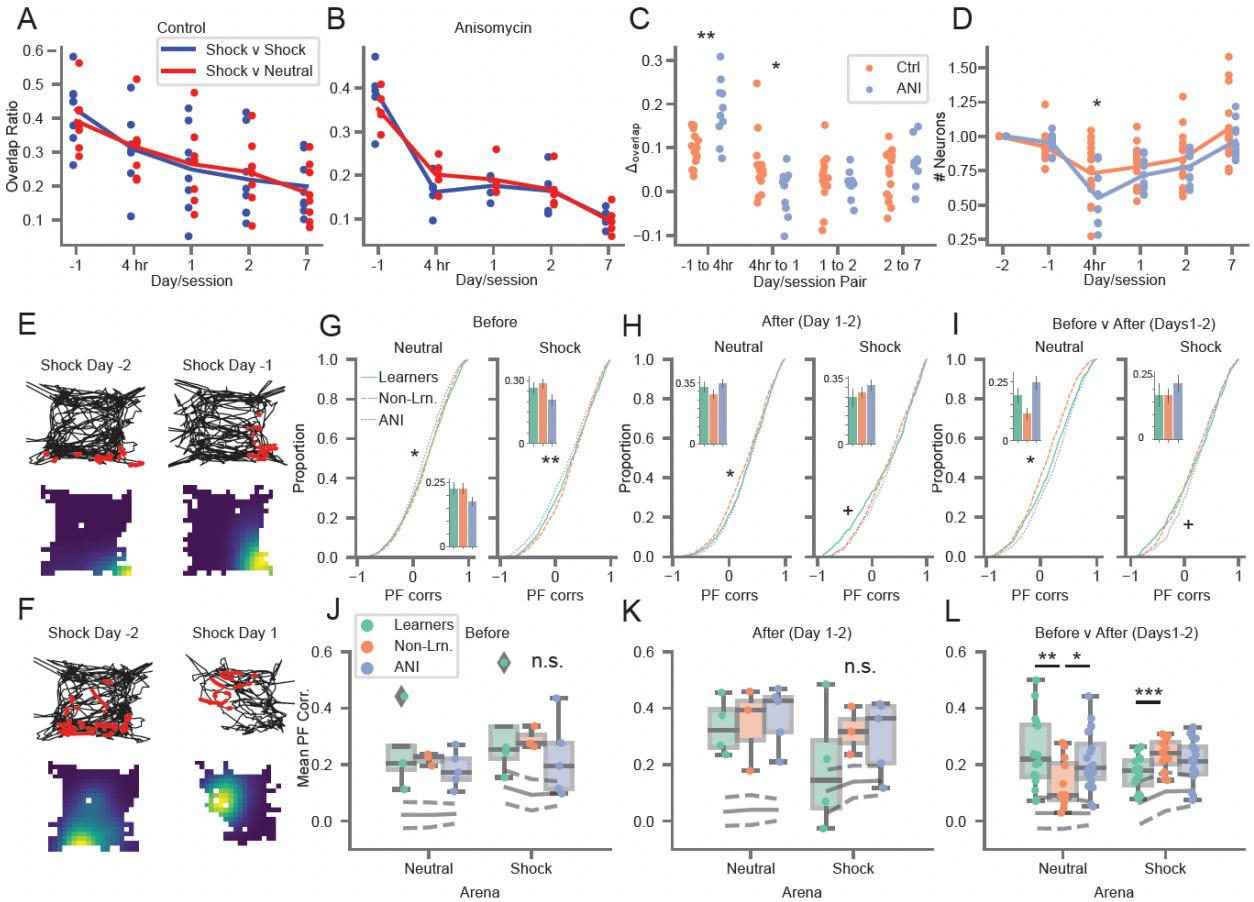

Figure 2: Anisomycin accelerates cell turnover and stifles learning-related place field remapping. A) Cell overlap ratio with Day -2 session, Control mice. Blue = within shock arena, red = shock v. neutral arena. **B)** Same as A) but for anisomycin mice. **C)** Change in overlap ratios from a and b. *p=0.028, **p=0.00024 two-sided t-test **D)** Number of active neurons observed each day, normalized to day -1. *p=0.039 two-sided t-test **E)** Stable place field. (top) Example mouse trajectory (black) with calcium activity (red) overlaid for the same cell from day -2 to -1 in shock arena, (bottom) occupancy normalized rate maps for the same cells **F)** Same as E) but for a different cell that remaps from day -2 to day 1 in the shock arena. **G)** Place field correlations for all mice before shock (Days -2 and -1). *p<0.0032 Learners vs ANI and Non-Learners vs ANI, **p=1.9e-6 Non-Learners vs ANI, k-s test after Bonferroni correction. **H)** Same as G) but for days after shock. *p=0.045 Learners vs Non-Learners and p=0.0059 Non-Learners vs ANI, +p=0.1 Learners vs ANI **I)** Same as G) but to assess learning-related remapping from before to after shock. *p=0.00021 Learners vs Non-Learners and p=3.4e-11 Non-Learners vs ANI, +p=0.12 Learners vs ANI **J)** Place field correlations before shock broken down by mouse **K)** Same as J) but for sessions after shock L) Same as J) but from before to after shock. p=0.002 mixed ANOVA, group x arena interaction. *p=0.025 Non-Learners vs ANI, **p=0.013 Learners vs Non-Learners, ***p=0.034 Learners vs ANI, post-hoc pairwise t-test after Bonferroni correction.

Next, we examined how blocking memory consolidation stopped learning-related remapping. We hypothesized that, by limiting long-term but not short-term synaptic plasticity, ANI administration would prevent learning-related remapping and stabilization of place fields following shock (Moita et al., 2004; Wang et al., 2012). To that end, we assessed place field remapping within and across epochs by comparing event rate maps for all neurons active between two sessions (Figure 2E-F). We noticed that the Learners group exhibited very low correlations in the Neutral arena throughout the experiment (Figure S3), which could indicate remapping. However, low correlations could occur not due to remapping but to errors in alignment of the entire place field map, which happen when an animal's place fields all rotate to the same degree around a single point as if the animal confused west for north (Keinath et al., 2017; Kinsky et al., 2018). Importantly, between-cell firing relationships are maintained following coherent map rotations. To disentangle these two possibilities, we rotated all maps from one session together in 90 degree increments and found the correlation that produced the highest

correlation between sessions. After accounting for coherent rotations in this manner, we found a robust increase in correlations for Learners but not for the other groups (Figure 2G-H, J-K vs. Figure S3), indicating that Learner place fields maintained a stable, but rotationally inconsistent, configuration between session. We thus performed all following analyses using the rotation that produced the highest correlation. We found that, despite small differences between groups (Figure 2G-H), all place field correlations were above chance (Figure 2J-K) both before and after learning, though Learners trended toward lower stability after shock (Figure 2H, K). We then compared place fields from before-shock to after-shock to assess learning-related remapping. In agreement with previous studies (Moita et al., 2004; Wang et al., 2012), Learner place fields remapped, as indicated by lower correlations in the Shock arena compared to the other gropus (Figure 2I, L). Interestingly, Non-Learners exhibited lower correlations than the other groups in the Neutral arena, indicated place field stability in the Shock arena and remapping in the Neutral arena (Figure 2I, L). If learning causes remapping, this double dissociation suggests that Non-Learner memory deficits might result from improperly associating the Neutral arena with shock. In contrast, the ANI group displayed high correlations throughout, indicating that learning-related remapping requires protein synthesis to stabilize the set of place fields which remap to support memory consolidation. This result indicates that remapping in the Shock arena is necessary for creation of a specific contextual fear memory and that a lack of remapping or improperly remapping in the Neutral arena may underlie the memory deficits observed in Non-Learner and the ANI group.

In addition to the aforementioned spatial coding, hippocampal neural activity also reflects non-spatial, task-related variables (McKenzie et al., 2014; Muzzio et al., 2009; Wood et al., 1999). We noticed that many hippocampal neurons exhibited calcium activity immediately before a mouse froze (Figure 3A-B, Figure S6A-C). Neurons which exhibited a significant increase in calcium event probability +/- 2 sec from a freezing epoch we therefore dubbed freeze-tuned cells (Figure 3D-F) in line with recent studies (Lee & Han, 2022; Schuette et al., 2020). Despite observing similar proportions across all groups and recording sessions (Figure 3C, Figure S6D), we noticed that freeze-tuned cells appeared to activate more reliably around freezing epochs following learning for Learners compared to Non-Learners and the ANI group (Figure 3D-E vs. Figure 3F and Figure S6B-C). This suggests that before learning, the neuronal population maintained a subset of immobility signaling cells (Kay et al., 2016) which changed from day to day and gained more reliable freeze-tuning after learning.

To test this possibility, we tracked the peak, peri-freeze event probability of each freeze cell backwards and forwards in time from the 4 hour recall session. Surprisingly, freeze-cell reliability did not significantly change for any group from before learning to after (Figure 3G). However, when we tracked cells backward/forward from the day 1 recall session, we found that Learner freeze cells exhibited much higher tuning stability than the other groups from the 4 hour to day 1 sessions (Figure 3H). This suggests that the subset of Learner neurons which exhibit freeze-tuned activity shortly after learning maintain this tuning during long term memory recall; in contrast, freeze cells from ANI group and Non-Learners are more transient and unreliable from 4 hours to 1 day post learning.

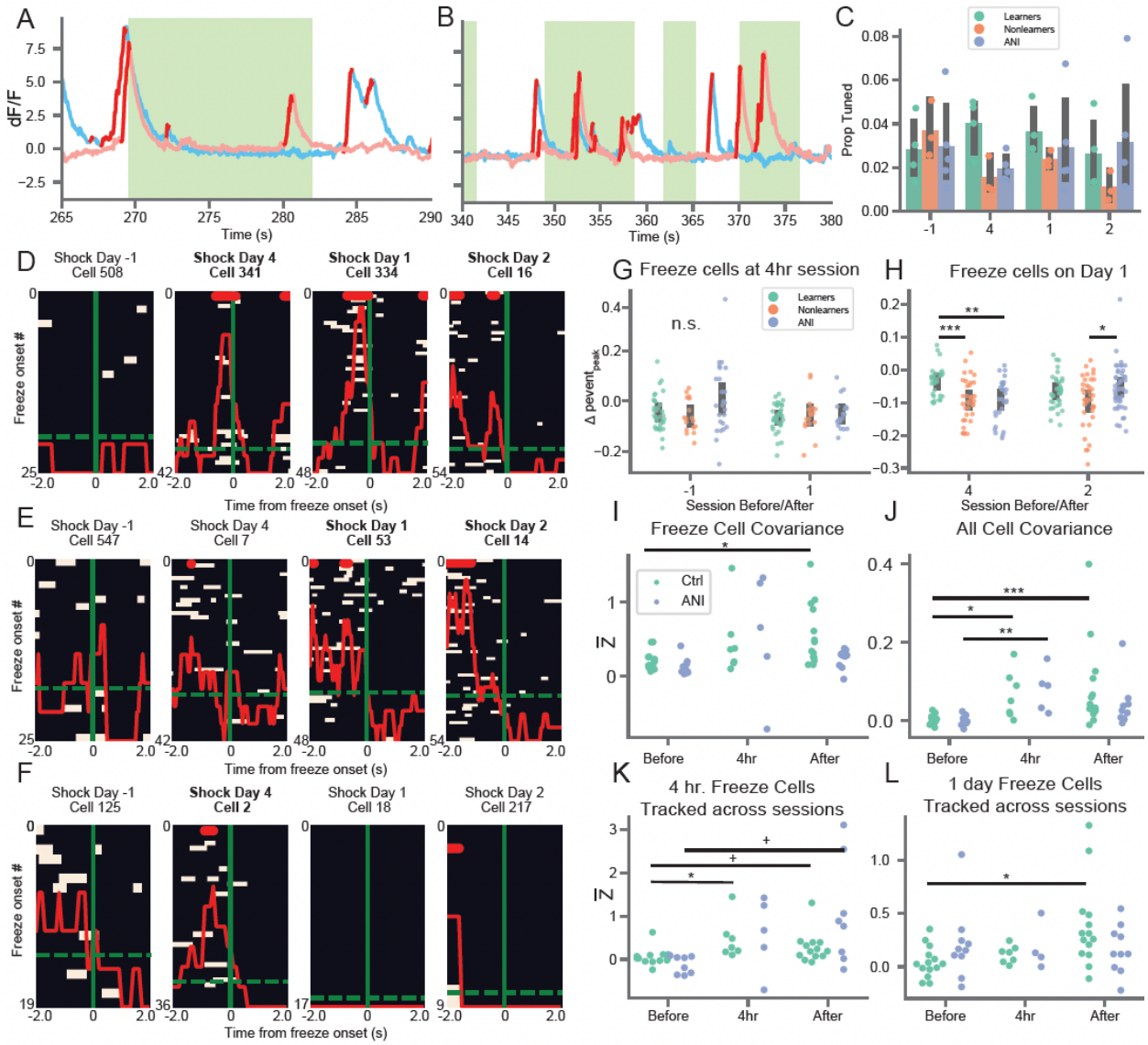

Figure 3: ANI administration suppresses the development of coordinated freeze-related neural activity. A) and B) Example traces from two freeze-cells which exhibit coordinated activity prior to freezing event during the Day 1 memory recall session in the shock arena, red = putative spiking activity. Pink = cell shown in C, blue = cell shown in E. **C)** Proportion of freeze-tuned cells detected each day across all groups. Green = freezing epochs. **D) and E)** Example Learner freeze-tuned cells identified on shock day 1 (bold) tracked across sessions. Peri-event calcium activity rasters are centered on freeze onset time (solid green). Dashed green = baseline calcium event probability, red solid = peri-freeze calcium event probability, bins with p<0.01 (circular permutation test) noted with red bars at top. D/E corresponds to pink/blue cells shown in A-B. **F)** Same as D and E but for ANI mouse shock cell identified during the 4 hour session. **G)** Change in peak peri-freeze calcium event probability for all freeze-tuned cells detected during the 4 hour session. **H)** Same as G but for freeze-tuned cells detected during Day 1 recall session. p < 0.02 1-way ANOVA each day separately, *p=0.02, **p=0.001, ***p=0.0006 post-hoc Tukey test. **I)** Freeze-tuned cells exhibit increased covariance in the Control compared to the ANI group. Mean covariance of freeze-tuned cells from each session shown. p=0.016 two-way ANOVA (Time). *p=0.018 post-hoc pairwise t-test (two-sided) after Bonferroni correction. **J)** Small but significant increase in covariance of all cells for Control mice during the 1 day recall session. p=0.0015 (Time), 0.005 (Group), 0.036 (Group x Time) two-way ANOVA. *p=0.014, **p=0.008, ***p=0.004 post-hoc pairwise t-test (two-sided) after Bonferroni correction. **K)** Mean covariance of freeze-tuned cells detected during the 4 hour session tracked across sessions. P=0.005 (Group), 0.04 (Group x Time) two-way ANOVA. p=0.014, +p=0.09 post-hoc pairwise t-test (two-sided) after Bonferroni correction. **L)** Same as K but for freeze-tuned cells detected during Day 1 recall session. p=0.0003 (Group) two-way ANOVA. *p=0.016 post-hoc pairwise t-test (two-sided) after Bonferroni correction.

Last, we investigated whether this increased reliability translated to increased freeze-tuned cell co-activity. Freeze-cell covariance increased gradually at the 4 hour session for all mice;

covariance remained high on days 1 and 2 for Control mice (Learner and Non-Learners combined) but returned to baseline for the ANI group (Figure 3I). This effect held when considering the covariance of all cells (Figure 3J) and was driven by increased covariance for Learners but not Non-Learners (Figure S6J-K). We observed similar results when we downsampled the number of freezing events following learning to match that on days -2 and -1 (Figure S6F-G). For freeze cells, but not all cells, this increased covariance was driven by peri-freeze neural activity (Figure S6H-I). These analyses utilized freeze-cells identified independently on each day of the experiment. We found that freeze-tuned cells identified on day 1 and tracked across days exhibited increased covariance on days 1 and 2 for the Control, but not the ANI group (Figure 3L). However, these cells did not increase their covariance during the 4 hour session, suggesting that though freeze-tuning begins to emerge immediately following learning cell connections continue to reorganize up to one day later to form coordinated ensembles. Freeze-cells identified at the 4 hour session displayed increased covariance for the Control, but not the ANI group (Figure 3K). These results indicate that freeze-related tuning emerges immediately following learning and continues to take shape for up to 24 hours. Additionally, this process requires protein synthesis to sharpen peri-freeze tuning and form individual cells into a coordinated, freeze-tuned ensemble.

Our results provide evidence that HPC spatial representations support contextual memory formation and consolidation. We speculate that the brain's ability to form distinct representations of two arenas with overlapping contextual qualities predisposes it to form discrete contextual memories and could underlie why some mice learn while others do not. Between-arena neural overlap correlated strongly with across-day neural overlap (Figure 1E), suggesting that the neural basis for contextual discrimination and representational drift may share the same mechanism (Hainmueller & Bartos, 2018; Kinsky et al., 2020; Mankin et al., 2012). Conversely, the similarity of neural representations after learning can serve as a biological signature of the degree of memory generalization. Moreover, anisomycin acutely suppressed neural activity in a subset of cells following learning (Figure 2D, Figure S7). This suggests that arresting protein synthesis in a subset of cells, perhaps those undergoing remapping, may temporarily reduce their activity rate by preventing the strengthening of new connections. Alternatively, reduced activity could result from blocking constitutive protein translation (Scavuzzo et al., 2019). However, our study does not support this view as we did not observe a global shutdown of neural activity but rather a decrease of activity in a subset of cells (Figure 2D, Figure S7). Despite this suppression, anisomycin's amnestic effects coincide with a reduction in learning-related neural reorganization, effectively halting HPC contextual representations in their prior state. Last, we confirm that a subset of hippocampal cells exhibits freeze tuning following fear conditioning (Schuette et al., 2020). The covariance of these cells increases following learning (Lee & Han, 2022) and requires protein synthesis (Figure 3H-I).

Overall, our results indicate that protein synthesis is necessary for forming new, stable spatial representations of an aversive context following learning and for producing coordinated activity of freeze-tuned neurons. We also found that inherent neural variability in HPC neuron dynamics prior to learning impacts the specificity of contextual fear memory. Our finding that anisomycin suppresses neural activity in a subset of cells suggests that it not only prevents learning-related plasticity but also weakens the activity of neurons involved in learning, which is resonant with the notion that more excitable/active neurons are preferentially involved in memory trace formation (Rashid et al., 2016; Sweis et al., 2021). A previous study demonstrated that synchronous optogenetic stimulation of engram neurons tagged during learning could artificially

reactivate a fear memory even when normal long-term recall of the fear memory was blocked by anisomycin (Ryan et al., 2015). Our results provide a parsimonious explanation for these results by demonstrating that anisomycin injection post-learning halts the co-firing of freeze-tuned cells, potentially impairing their ability to transmit behavior-related information to downstream regions and impairing the ability to retrieve memories (Ryan & Frankland, 2022). Future work will disentangle the differential contributions that halting protein synthesis versus suppressing neural activity play in disrupting memory consolidation.

Acknowledgments: First and foremost, we would like to thank Howard Eichenbaum who helped conceive and design this study before his unfortunate passing in 2017. We would also like to thank Sam McKenzie for his help during early experimental design. We would like to thank Michael Hasselmo and Ian Davison for their support and feedback while performing the recordings for this study. Next, we thank Sam Levy, Dave Sullivan, and Will Mau for their assistance in all phases of calcium imaging throughout. We would like to thank Zach Pennington for valuable feedback concerning anisomycin preparation and administration, and Denise Cai and Lucas Carstensen for analysis suggestions. We would like to thank Pho Hale, Rachel Wahlberg, and Utku Kaya for feedback on the manuscript. We would like to acknowledge the GENIE Program, specifically Vivek Jayaraman, PhD, Douglas S. Kim, PhD, Loren L. Looger, PhD, Karel Svoboda, PhD from the GENIE Project, Janelia Research Campus, Howard Hughes Medical Institute, for providing the GCaMP6f virus. Finally, we would like to acknowledge Inscopix, Inc. for making single-photon calcium imaging miniscopes widely available, and specifically Lara Cardy and Vardhan Dani for all their technical support throughout the experiment. This work was supported by NIH Grants R01 MH052090, R01 MH051570, R01MH117964, NIH NRSA Fellowship 1F32NS117732-01, NIH Early Independence Award DP5 OD023106-01, an NIH Transformative R01 Award, a Young Investigator Grant from the Brain and Behavior Research Foundation, a Ludwig Family Foundation grant, and the McKnight Foundation Memory and Cognitive Disorders award, and Boston University's Neurophotonics Center,

References

Agnihotri, N. T., Hawkins, R. D., Kandel, E. R., & Kentros, C. G. (2004). The long-term stability of new hippocampal place fields requires new protein synthesis. Proceedings of the National Academy of Sciences, 101(10), 3656–3661. https://doi.org/10.1073/pnas.0400385101

Barondes, S. H., & Cohen, H. D. (1967). Delayed and Sustained Effect of Acetoxycycloheximide on Memory in Mice. Proceedings of the National Academy of Sciences of the United States of America, 58, 157–164.

Cai, D. J., Aharoni, D., Shuman, T., Shobe, J., Biane, J., Lou, J., Kim, I., Baumgaertel, K., Levenstain, A., Tuszynski, M., Mayford, M., & Silva, A. J. (2016). A shared neural ensemble links distinct contextual memories encoded close in time. Nature, 534, 115–118. https://doi.org/10.1038/nature17955

Cohen, H. D., & Barondes, S. H. (1966). Puromycin and Cycloheximide: Different Effects on Hippocampal Electrical Activity. Science, 154(3756), 1557–1558. https://doi.org/10.1126/science.154.3756.1557

Frey, U., & Morris, R. G. M. (1998). Synaptic tagging: Implications for late maintenance of hippocampal long- term potentiation. Trends in Neurosciences, 21(5), 181–188. https://doi.org/10.1016/S0166-2236(97)01189-2

Ghosh, K. K., Burns, L. D., Cocker, E. D., Nimmerjahn, A., Ziv, Y., Gamal, A. el, & Schnitzer, M. J. (2011). Miniaturized integration of a fluorescence microscope. Nature Methods, 8(10), 871–878. https://doi.org/10.1038/nmeth.1694

Hainmueller, T., & Bartos, M. (2018). Parallel emergence of stable and dynamic memory engrams in the hippocampus. Nature, 558(7709), 292–296. https://doi.org/10.1038/s41586-018-0191-2

Keinath, A. T., Julian, J. B., Epstein, R. A., & Muzzio, I. A. (2017). Environmental Geometry Aligns the Hippocampal Map during Spatial Reorientation. Current Biology, 27(3). https://doi.org/http://dx.doi.org/10.1016/j.cub.2016.11.046

Kinsky, N. R., Mau, W., Sullivan, D. W., Levy, S. J., Ruesch, E. A., & Hasselmo, M. E. (2020). Trajectory-modulated hippocampal neurons persist throughout memory-guided navigation. Nature Communications, 1–14. https://doi.org/10.1038/s41467-020-16226-4

Kinsky, N. R., Sullivan, D. W., Mau, W., Hasselmo, M. E., & Eichenbaum, H. B. (2018). Hippocampal Place Fields Maintain a Coherent and Flexible Map across Long Timescales. Current Biology, 28(22), 1–11. https://doi.org/10.1016/J.CUB.2018.09.037

Mankin, E. A., Sparks, F. T., Slayyeh, B., Sutherland, R. J., Leutgeb, S., & Leutgeb, J. K. (2012). Neuronal code for extended time in the hippocampus. Proceedings of the National Academy of Sciences, 109(47), 19462–19467. https://doi.org/10.1073/pnas.1214107109/-/DCSupplemental.www.pnas.org/cgi/doi/10.1073/pnas.1214107109

McKenzie, S., Frank, A. J., Kinsky, N. R., Porter, B., Rivière, P. D. P. D., & Eichenbaum, H. B. (2014). Hippocampal representation of related and opposing memories develop within distinct, hierarchically organized neural schemas. Neuron, 83(1), 202–215. https://doi.org/10.1016/j.neuron.2014.05.019

Moita, M. A. P., Rosis, S., Zhou, Y., LeDoux, J. E., & Blair, H. T. (2004). Putting Fear in Its Place: Remapping of Hippocampal Place Cells during Fear Conditioning. Journal of Neuroscience, 24(31), 7015–7023. https://doi.org/10.1523/JNEUROSCI.5492-03.2004

Muir, D. R., & Kampa, B. M. (2015). FocusStack and StimServer: a new open source MATLAB toolchain for visual stimulation and analysis of two-photon calcium neuronal imaging data. Frontiers in Neuroinformatics, 8(January), 1–13. https://doi.org/10.3389/fninf.2014.00085

Muzzio, I. A., Levita, L., Kulkarni, J., Monaco, J. D., Kentros, C. G., Stead, M., Abbott, L. F., & Kandel, E. R. (2009). Attention enhances the retrieval and stability of visuospatial and olfactory representations in the dorsal hippocampus. PLoS Biology, 7(6). https://doi.org/10.1371/journal.pbio.1000140

Rashid, A. J., Yan, C., Mercaldo, V., Hsiang, H. L., Park, S., Cole, C. J., Cristofaro, A. de, Yu, J., Ramakrishnan, C., Lee, S. Y., Deisseroth, K., Frankland, P. W., & Josselyn, S. A. (2016). Competition between engrams influences fear memory formation and recall. Science, 353(6297), 383–388. https://doi.org/10.1126/science.aaf0594

Resendez, S. L., Jennings, J. H., Ung, R. L., Namboodiri, V. M. K., Zhou, Z. C., Otis, J. M., Nomura, H., McHenry, J. A., Kosyk, O., & Stuber, G. D. (2016). Visualization of cortical, subcortical and deep brain neural circuit dynamics during naturalistic mammalian behavior with head-mounted microscopes and chronically implanted lenses. Nature Protocols, 11(3), 566–597. https://doi.org/10.1038/nprot.2016.021

Ryan, T. J., Roy, D. S., Pignatelli, M., Arons, A., & Tonegawa, S. (2015). Engram cells retain memory under retrograde amnesia. Science, 348(6238), 1007–1013. https://doi.org/10.1126/science.aaa5542

Scavuzzo, C. J., LeBlancq, M. J., Nargang, F., Lemieux, H., Hamilton, T. J., & Dickson, C. T. (2019). The amnestic agent anisomycin disrupts intrinsic membrane properties of hippocampal neurons via a loss of cellular energetics. Journal of Neurophysiology, 122(3), 1123–1135. https://doi.org/10.1152/jn.00370.2019

Sharma, A. v., Nargang, F. E., & Dickson, C. T. (2012). Neurosilence: Profound Suppression of Neural Activity following Intracerebral Administration of the Protein Synthesis Inhibitor Anisomycin. The Journal of Neuroscience, 32(7), 2377–2387. https://doi.org/10.1523/JNEUROSCI.3543-11.2012

Squire, L. R., & Barondes, S. H. (1973). Memory impairment during prolonged training in mice given inhibitors of cerebral protein synthesis. Brain Research, 56(C), 215–225. https://doi.org/10.1016/0006-8993(73)90336-3

Sweis, B. M., Mau, W., Rabinowitz, S., & Cai, D. J. (2021). Dynamic and heterogeneous neural ensembles contribute to a memory engram. Current Opinion in Neurobiology, 67, 199–206. https://doi.org/10.1016/j.conb.2020.11.017

Wang, M. E., Wann, E. G., Yuan, R. K., Ramos Álvarez, M. M., Stead, S. M., & Muzzio, I. A. (2012). Long-term stabilization of place cell remapping produced by a fearful experience. The Journal of Neuroscience, 32(45), 15802–15814. https://doi.org/10.1523/JNEUROSCI.0480-12.2012

Wiltgen, B. J., Zhou, M., Cai, Y., Balaji, J., Karlsson, M. G., Parivash, S. N., Li, W., & Silva, A. J. (2010). The hippocampus plays a selective role in the retrieval of detailed contextual memories. Current Biology : CB, 20(15), 1336–1344. https://doi.org/10.1016/j.cub.2010.06.068

Wood, E. R., Dudchenko, P. A., & Eichenbaum, H. B. (1999). The global record of memory in hippocampal neuronal activity. Nature, 397(6720), 613–616. https://doi.org/10.1038/17605

Methods:

Animals

Sixteen (n = 10 controls, 6 anisomycin) male C57/BL6 mice (Jackson Laboratories), age 16 to 22 weeks during behavioral and imaging experiments and weighing 25-32g were used in this study. Three mice were excluded after performing this study: one mouse after histology revealed the GRIN lens implant and viral expression to be medial to the intended imaging, while the other two were excluded due to unstable/overexpression of GCaMP that produced aberrant calcium activity which emerged toward the end of the experiment. After exclusion of these mice, we retained 8 control mice and 5 anisomycin mice. Additionally, behavioral video tracking files for one control mouse were corrupted during recording during all neutral field recordings from day 0 on: this mouse was excluded from all analyses which required using behavior in the Neutral arena (e.g., place field correlations and any analyses where the control group was split into Learners and Non-Learners). Mice were socially housed in a vivarium on a 12 hour light-dark cycle with 1-3 other mice prior to surgery and were housed singly thereafter. Mice were given free access to food and water throughout the study. All procedures were performed in compliance with the guidelines of the Boston University Animal Care and Use Committee.

One male Long Evans rat, 10 months old and weighing ~480g, was used for the electrophysiological recording in this study. Rats were socially housed in a vivarium on an adjusted 12 hour light-dark cycle (lights on at noon, off at midnight) with 1-3 other rats prior to surgery and given free access to food and water throughout the study. All procedures were performed in compliance with the guidelines of the University of Michigan Animal Care and Use Committee.

Viral Constructs

For mice experiments we used an AAV9.*Syn*.GCaMP6f.WPRE.SV40 virus from the University of Pennsylvania Vector Core/Addgene with an initial titer of ~$4x10^{12}$ GC/mL and diluted it into sterilized potassium phosphate buffered saline (KPBS) to a final titer of ~$2\text{-}4x10^{12}$ GC/mL for injection.

For rat experiments, we used an pGP.AAV9.*Syn*.GCaMP7f.WPRE.SV40 virus from the University of Pennsylvania Vector Core/Addgene with an initial titer of $2.6x10^{13}$ GC/mL and diluted it into sterilized phosphate buffered saline (PBS) to a final titer of $2.6x10^{12}$ GC/mL for injection. Due to poor expression no imaging was performed.

Stereotactic Surgery

We performed two stereotactic surgeries and one base-plate implant on naïve mice, aged 3-8 months, according to previously published procedures (Kinsky et al., 2018; Resendez et al., 2016). Both surgeries were performed under 1-2% isoflurane mixed with oxygen. Mice were given 0.05mL/kg buprenorphine (Buprenex) for analgesia (subcutaneously, SC), 5.0mL/kg of the anti-inflammatory drug Rimadyl (Pfizer, SC), and 400mL/kg of the antibiotic Cefazolin (Pfizer, SC) immediately after induction. They were carefully monitored to ensure they never dropped below 80% of their pre-operative weight during convalescence and received the same dosage of Buprenex, Cefazolin, and Rimadyl twice daily for three days following surgery. In the first surgery, a small craniotomy was performed at AP -2.0, ML +1.5 (right) and 250nL of

367 GCaMP6f virus (at the titer noted below) was injected 1.5mm below the brain surface at
368 40nL/min using a 1μL Hamilton syringe and infusion pump. The needle remained in place a
369 minimum of 10 minutes after the infusion finished at which point it was slowly removed, the
370 mouse's scalp was sutured, and the mouse was removed from anesthesia and allowed to
371 recover.

372 3-4 weeks after viral infusion, mice underwent second surgery to attach a gradient index (GRIN)
373 lens (GRINtech, 1mm x 4mm). After performing an ~2mm craniotomy around the implant area,
374 we carefully aspirated cortex using blunted 25ga and 27ga needles under constant irrigation
375 with cold, sterile saline until we visually identified the medial-lateral striations of the corpus
376 callosum. We carefully removed these striations using a blunted 31ga needle while leaving the
377 underlying anterior-posterior striations intact, after which we applied gelfoam for 5-10 minutes to
378 stop any bleeding. We then lowered the GRIN lens to 1.1mm below bregma. Note that this
379 entailed pushing down ~50-300μm to counteract brain swelling during surgery. We then applied
380 Kwik-Sil (World Precision Instruments) to provide a seal between skull and GRIN lens and then
381 cemented the GRIN lens in place with Metabond (Parkell), covered it in a layer of Kwik-Cast
382 (World Precision Instruments), and then removed the animal from anesthesia and allowed him
383 to recover after removing any sharp edges remaining from dried Metabond with a dental drill
384 and providing any necessary sutures.

385 Finally, after ~2-4 weeks we performed a procedure in which the mouse was put under
386 light anesthesia to attach a base plate for easy future attachment of a miniature epifluorescence
387 microscope (Ghosh et al., 2011, Inscopix, Inc.). Importantly, no tissue was cut during this
388 procedure. After induction, we attached the base plate to the camera via a set screw, set the
389 camera's focus level at ~1/3 from the bottom of its range, and carefully lowered the camera
390 objective and aligned it to the GRIN lens by eye, and visualized fluorescence via nVistaHD until
391 we observed clear vasculature and putative cell bodies expressing GCaMP6f (Resendez et al.,
392 2016). To counteract downward shrinking during curing, we then raised the camera up ~50μm
393 before applying Flow-It ALC Flowable Composite (Pentron) between the underside of the
394 baseplate and the cured Metabond on the mouse's skull. After light curing, we applied opaque
395 Metabond over the Flow-It ALC epoxy to the sides of the baseplate to provide additional
396 strength and to block ambient light infiltration. Mice were allowed to recover for several days
397 prior to habituation to camera attachment and performance of the behavioral task outlined
398 below. In the event that we did not observe clear vasculature and cell bodies when we first
399 visualized fluorescence we covered the GRIN lens with Kwik-Cast and removed the mouse from
400 anesthesia without attaching the baseplate. We then waited an additional week and repeated
401 the steps above.

402 For rats, we performed two surgeries in a similar manner as described above for mice.
403 However, rats were administered pre-operative and post-operative Meloxicam orally for
404 analgesia (in lieu of Buprenex) and triple-antibiotic was applied locally (in lieu of Cefazolin
405 injections) to the incision at the end of surgery. Meloxicam was additionally administered for two
406 days post-surgery during recovery, and animals were monitored daily for a minimum of seven
407 days during recovery. 0.4mL of a lidocaine/bupivacaine cocktail were given under the scalp to
408 provide local anesthesia at the incision site. In the first surgery, 1000nL of GCaMP7f virus was
409 infused in the prelimbic cortex at the center of a 1mm craniotomy (AP + 2.9, ML + 3.6, from
410 Bregma, DV -3.0 at an 18 degree angle from top of brain). Following infusion, ~1.5 mm of
411 overlying cortex was removed and a 23ga needle was lowered to ~500μm above the target site.

412 Then, a 0.6 x 7 mm GRIN lens was lowered to 3.0mm below the top of the brain, the area
413 between the skull and lens was sealed with Kwik-Sil, and the lens was affixed to the skull with
414 Vivid-Flow light-curable composite (Pearson Dental) and Metabond (Parkell). The lens was
415 then covered in Kwik-Sil for protection. During this surgery, ground and reference screws were
416 also placed over the cerebellum and a 3d printed crown base was attached to the rat's skull
417 (Vöröslakos et al., 2021) to which crown walls and top were connected and to further protect the
418 lens and future microdrive/probe implant. The rat was screened for fluorescence 8-12 weeks
419 later, but no cell dynamics were observed so no imaging equipment was implanted for this rat.

420 16 weeks later, the rat was again given pre-operative Meloxicam and anesthetized under
421 isoflurane. The crown walls were removed and a 1.0mm craniotomy was performed at AP-4.8,
422 ML+3.6 from bregma. After removing dura and stopping bleeding with cold, sterile saline, a
423 NeuroNexus A1x32-5mm-50-177 probe, attached to a metal microdrive, was implanted at 2.3
424 mm below the brain surface and the metal drive base was attached to the skull with Unifast light
425 cured dental epoxy (Henry-Schein). The craniotomy was sealed with Dow-Sil, the probe was
426 protected with dental wax, and the ground and reference wires were connected to the probe
427 electronic interface board (EIB). The crown walls were re-attached, the EIB was connected to
428 the crown walls, and the rat was removed from isoflurane and allowed to recovery. The rat was
429 monitored daily for 7 days prior to recording, during which the probe was lowered ~1mm until
430 sharp wave ripples and spiking activity were visualized indicating localization of the probe in the
431 CA1 cell layer.

432 **Histology procedures**

433 Hippocampal slices were prepared following extraction from mice in accordance with the
434 standard methods and guidelines of the Boston University Animal Care and Use Committee. In
435 brief, mice were euthanized with Euthasol (Virbac), transcardially perfused with
436 paraformaldehyde (PFA), and decapitated. Following extraction, brains were placed in PFA for
437 approximately 48 hours before undergoing sectioning. Brains that were sliced using a Cryostat
438 underwent an additional step of sucrose cryoprotection and subsequent freezing in -80C. Brains
439 were mounted to the slicing platform using Tissue Tek O. C. T. (Sakura) and kept at -30C
440 throughout sectioning. 50µm slices were collected across the entire aspiration site in the dorsal
441 hippocampus region. Brains that were sliced using a vibratome were stabilized using super glue
442 and submerged in 1% PBS. A Leica VT1000 S vibratome was equipped with a platinum coated
443 double edged blade (Electron Microscopy Sciences , Cat. #72003-01) and set to a maximal
444 speed of 0.9mm/s for collecting 50 µm slices. Slices prepared from both the cryostat and
445 microtome were directly mounted onto (type of slides go here) and cover-slipped using DAPI
446 following sectioning. No histology was performed in the rat study.

447 **Behavioral Paradigm**

448 Prior to surgery mice were handled to habituate them subsequent camera attachment. 3-7 days
449 following base plate attachment surgery we conditioned mice to the imaging procedures by
450 further handling them for 5-10 minutes for a minimum three days. During this handling a plastic
451 "dummy" microscope (Inscopix) of approximately the same size/weight as the imaging camera
452 was attached to each mouse's head and remained on his head for 1-2 hours in his home cage.
453 When it became easy to attach the scope to the mouse's head a real imaging miniscope was
454 attached to head and an optimal focus plane chosen. We then recorded three 5 minute imaging
455 videos at this focus and +/- ¼ turn (~25µm) in the mouse's home cage. These movies were

processed as described in the Image Acquisition and Processing section and an optimal zoom was chosen based on whichever focus plane maximized cell yield and produced clear looking cell bodies. Animals were then placed in a novel environment with a different size and shape compared to the experimental environments for a 10 minute session to habituation them to the general experimental outline and ensure that they explored novel arenas.

Following habituation to the imaging procedures mice performed a contextual fear conditioning (CFC) task with simultaneous imaging of hippocampus neurons over the course of 10 days. Note that all recording sessions are referred to by their time relative to applying the mild foot-shock and the arena in which the recording occurred: e.g., SHOCK Day -2 occurred in the SHOCK arena two days prior to foot-shock while NEUTRAL 4 hours occurred four hours after foot-shock in the neutral arena. A typical day (Days -2, -1, 1, 2, and 7) consisted of two separate 10 minute recording blocks/sessions: one in the NEUTRAL arena and one in the SHOCK arena. Mice first explored a square (NEUTRAL) arena, placed in the center of a well-lit room, for 10 minutes. The NEUTRAL arena was a square constructed of 3/8” plywood (25cm x 25cm x 15 cm), which was painted yellow with sealable paint. Additionally, one wall was painted with black horizontal stripes for visual orientation purposes. The NEUTRAL arena was wiped down with 70% ethanol ~10 minutes prior to recording. After 10 minutes of exploration the experimenter took the mouse out of the arena, leaving the miniscope camera on their head and placed the mouse in its home cage on a moveable cart upon which it was immediately transported down a short hallway to second room.

The second room was dimly lit and contained the fear conditioning (SHOCK) arena. The SHOCK arena (Coulbourn Instruments, Whitehall, PA, USA) consisted of metal-panel side walls, Plexiglas front and rear walls, and a stainless-steel grid floor composed of 16 grid bars (22cm x 22cm). Following 10 minutes of exploration of the SHOCK arena, mice were removed from the arena, the camera was removed, and mice were returned to their home cage. Both arenas were wiped down with 70% ethanol ~10min prior to recording to eliminate any odor cues. Note that mice always explored the NEUTRAL arena first and the SHOCK arena second. For the Day 0 sessions, mice first explored the NEUTRAL arena for 10 minutes and were transported to the SHOCK arena as usual. However, during this session (SHOCK Day 0) the mouse was immediately given a single 0.25mA shock and allowed to explore the arena for an additional 60 seconds only before being removed and returned to his cage. Efficacy of shock was confirmed post-hoc by eye by the presence of jumping/darting behavior immediately post-shock. The 4 hour session was identical to the Day -2, 1, 1, 2, and 7 sessions. With the exception of the 4 hour session, all recording sessions were performed in the first half of the mouse’s life cycle while the 4 hour session occurred in the second half of the light cycle.

On day zero, after the camera was removed and prior to returning to their home cage, mice received an intraperitoneal injection of either anisomycin (150 mg/kg, Sigma-Aldrich A9789) or the equivalent amount of vehicle. After injection, they were returned to their cage for 4 hours until the next recording session began.

Following extensive habituation to a rest box during the seven day recovery period, rat neural activity and behavior was recorded across ~ 5 hours. Following a 15 minute baseline recording (PRE) in the rest box, the animal was given an I.P. injection of anisomycin and then immediately placed on a novel linear track which he explored for 45 minutes (TRACK). The rat was then placed back into the rest box for 3.5 hours (POST). Following that, the animal was placed on a second novel track for 45 minutes (TRACK) followed by a brief recording in the rest box

(POST2). Data was acquired continuously throughout with the exceptions of periodic cable disconnections to perform the I.P. injection, start a new recording epoch, and disconnect/reconnect cables that became twisted.

Anisomycin

For mice recordings, 25 mg of anisomycin was dissolved into 50 µL of 6N HCl and 500 µL of 1.8%NaCl. ~125 µL of 1N NaOH was then added to the solution followed by 0.1-0.5 µL of 1N NaOH, testing pH after each addition until a final pH of 7.0 to 7.5 was reached, with a final concentration of 24-27 mg/mL. In the case that pH rose above 7.5 during titration and and/or the anisomycin went back into precipitate, small amounts (10-20 µL) of 6N HCl were added until particles were no longer visible and the titration with 1N NaOH was restarted. Mice were administered 150mg/kg of anisomycin solution via intraperitoneal injection, or ~0.15-0.18mL for a typical 30g mouse.

For rat recordings, 100mg of anisomycin was dissolved into 1.6mL of 0.1N HCl (in 0.9% saline). ~240 µL of 1N HCl was added, then 10-12 µL of NaOH was added in 1-2 µL amounts, testing pH between each step until a pH of 7-7.5 was reached. 0.9% Saline was then added until a final concentration of 33 mg/mL was reached. Due to a small amount of waste, the final amount injected was 50mg (1.5 mL) which corresponds to 100 mg/kg for the rat.

Behavioral Tracking and Fear Metrics

We utilized two different camera/software configurations for tracking animal behavior. Both configurations generated a TTL pulse at the beginning of behavioral tracking to synchronize with image acquisition. We utilized Cineplex software (v2, Plexon) to track animal location at 30Hz in the NEUTRAL arena. We used FreezeFrame (Actimetrics) to track animal location in the SHOCK arena at 3.75Hz. Animal location was obtained post-hoc via custom-written, freely available Python software (www.github.com/wmau/FearReinstatement). We observed inconsistent frame rates and inaccurate acquisition of behavioral video frames for one mouse in the NEUTRAL arena during the day 0, 4 hour, and day 1-2 sessions. These sessions were excluded from analysis.

Freezing was calculated by first dowsampling NEUTRAL position data to 3.75 Hz to match the sample rate used in the SHOCK arena. We then identified freezing epochs as any periods of 10 consecutive frames (2.67 seconds) or more where the mouse's velocity was less than 1.5cm/second.

Neural Discrimination

We evaluated the extent to which each animal's behavior reflected the expression of a context-specific fear memory through a behavioral discrimination index (DI_{Frz}), calculated as follows:

$$DI_{Frz} = \frac{Frz_{Neutral} - Frz_{Shock}}{Frz_{Neutral} + Frz_{Shock}}$$

Where $Frz_{Neutral}$ and Frz_{Shock} are the percentages of time spent freezing in the NEUTRAL and SHOCK arenas, respectively. Thus, a negative DI_{Frz} value indicated more freezing behavior in the shock arena (suggesting successful encoding of a context-specific fear memory), a positive DI_{Frz} value indicated more freezing behavior in the neutral arena, and a DI_{Frz} value around zero

indicated equal/low freezing behavior in each arena (suggesting the formation of a non-specific or weak fear memory).

Imaging Acquisition and Processing

Brain imaging data was obtained using nVista HD (Inscopix) at 720 x 540 pixels and a 20 Hz sample rate. Note that imaging data for one mouse was obtained at 10 Hz. Prior to neuron/calcium event identification we first pre-processed each movie using Inscopix Imaging Suite (Inscopix) software. Preprocessing entailed three steps a) motion corrections, and b) cropping the motion-corrected movie to eliminate any dead pixels or areas with no calcium activity, and c) extracting a minimum projection of the pre-processed movie for later neuron registration. We did not analyze one imaging session in which we had to reconnect the camera cable mid-session and could not synchronize the imaging data with behavioral data. Maximum projections of imaging movies were made using the Inscopix Imaging Suite or custom-written functions based off of an open-source MATLAB library (Muir & Kampa, 2015).

Electrophysiological Recordings

Data was acquired using an Intan 1028 channel recording system through OpenEphys software into binary format and behavior was tracked via Omnitrack high resolution cameras.

Data Analysis

Data analysis was performed in both Python and MATLAB software. Python analysis code is available at https://github.com/nkinsky/Eraser.

Spike sorting and analysis

Electrophysiological recordings were automatically clustered using SpyKING CIRCUS software (Yger et al., 2018) and units were manually curated in phy. Units were grouped into single units if they exhibited a clear refractory period and were well-isolated from other putative spikes. Other units which exhibited a clear waveform but were either poorly isolated or exhibited refractory period violations were classified as multi-unit activity (MUA). All single units and MUA were combined and cross-correlograms for the combined activity were created for each epoch of the recording separately.

Tenaspis

Neuron regions-of-interest (ROIs) and calcium events were identified using a custom written, open source algorithm employed in MATLAB 2016b called A Technique for Extracting Neuronal Activity from Single Photon Neuronal Image Sequences (Tenaspis) (Mau et al., 2018). This procedure was comprehensively documented in Kinsky et al., 2018:

"Tenaspis is open-source and available at: https://github.com/SharpWave/TENASPIS. First, Tenaspis filters each calcium imaging movie with a band-pass filter per (Kitamura et al., 2015) to accentuate the separation between overlapping calcium events. Specifically, Tenaspis smooths the movie with a 4.5 μm disk filter and divides it by another movie smoothed with a 23.6 μm disk filter. Second, it adaptively thresholds each imaging frame to identify separable pockets of calcium activity, designated as blobs, on each frame. Blobs of activity are accepted at this stage of processing only if they approximate the size and shape of a mouse hippocampal neuron, as measured by their radius (min = ~6μm, max = ~11μm), the ratio of long to short axes (max = 2), and solidity (min = 0.95), a metric used by the *regionprops* function of MATLAB we

581 employ to exclude jagged/strange shaped blobs. Third, Tenaspis strings together blobs on
582 successive frames to identify potential calcium transients and their spatial activity patterns.
583 Fourth, Tenaspis searches for any transients that could results from staggered activity of two
584 neighboring neurons. It rejects any transients whose centroid travels more than 2.5μm between
585 frames and whose duration is less than 0.20 seconds. Fifth, Tenaspis identifies the probable
586 spatial origin of each transient by constructing putative regions-of-interest (ROIs), defined as all
587 connected pixels that are active on at least 50% of the frames in the transient. Sixth, Tenaspis
588 creates initial neuron ROIs by merging putative transient ROIs that are discontinuous in time but
589 occur in the same location. Specifically, it first attempts to merge all ROIs whose centroids are
590 less than a distance threshold of ~0.6μm from each other. In order to merge two transient ROIs,
591 the two-dimensional Spearman correlation between the ROIs must yield $r^2 > 0.2$ and $p < 0.01$.
592 Tenaspis then successively increases the distance threshold and again attempts to merge ROIs
593 until no more valid merges occur (at a distance threshold of ~3μm, typically). Seventh, Tenaspis
594 integrates the fluorescence value of each neuron ROI identified in the previous step across all
595 frames to get that neuron's calcium trace, and then identifies putative spiking epochs for each
596 neuron. Specifically, it first identifies the rising epochs of any transients identified in earlier
597 steps. Then, it attempts to identify any missed transients as regions of the calcium trace that
598 have a) a minimum peak amplitude > 1/3 of the transients identified in step 3, b) a high
599 correlations ($p < 0.00001$) between active pixels and the pixels of the average neuron ROI
600 identified in step 6, and b) a positive slope lasting at least 0.2 seconds. Last, Tenaspis searches
601 for any neuron ROIs that overlap more than 50% and whose calcium traces are similar and
602 merges their traces and ROIs."

603 **Between Session Neuron Registration**

604 We utilized custom-written, freely available MATLAB code (available at
605 https://github.com/nkinsky/ImageCamp) to perform neuron registration across sessions in
606 accordance with previous results (Kinsky et al., 2018). The details of this procedure described in
607 Kinsky et al. (2018) are reproduced here:

608 "Neuron registration occurred in two steps: session registration and neuron registration.

609 *Session registration* - Prior to mapping neurons between sessions, we determined how
610 much the imaging window shifted between sessions. In order to isolate consistent features of
611 the imaging plane for each mouse (such as vasculature or coagulated blood), we created a
612 minimum projection of all of the frames of the motion-corrected and cropped brain imaging
613 movie for each recording session. One session ("registered session") was then registered to a
614 base session using the "imregtform" function from the MATLAB Image Processing Toolbox,
615 assuming a rigid geometric transform (rotation and translation only) between images, and the
616 calculated transformation object was saved for future use.

617 *Neuron Registration* - Next, each ROI in the registered session was transformed to its
618 corresponding location in the base session. Each neuron in the base session was then mapped
619 to the neuron with the closest center-of-mass in the registered session, unless the closest
620 neuron exceeded our maximum distance threshold of 3 pixels (3.3 μm). In this case the base
621 session neuron was designated to map to no other neurons in the registered session. If, due to
622 high density of neurons in a given area, we found that multiple neurons from the base session
623 mapped to the same neuron in the registered session, we then calculated the spatial correlation

(Spearman) between each pair of ROIs and designated the base session ROI with the highest correlation as mapping to the registered session ROI.

For multiple session registrations, the same procedure as above was performed for each session in two different ways. First, we registered each session directly to the first session in the experiment and updated ROI locations/added new ROIs to set of existing ROIs with each registration. This helped account for slight day-to-day drift in neurons ROIs due to shifts in vasculature, build-up of fluid underneath the viewing window, creep/shrinkage of dental cement, etc. Second, to ensure that neuron ROIs did not drift excessively across sessions we also performed all the above steps but did NOT update ROI locations allowing us to register each set of ROIs to those furthest away chronologically. The resulting mappings were then compared across all sessions, and any neuron mappings that differed between the two methods (e.g., ROIs that moved excessively across the duration of the experiment) were excluded from analysis. Those that remained in the same location were included."

The procedure to assess the quality of across session registration was described in Kinsky et al. (2018) and is reproduced here: "We checked the quality of neuron registration between each session-pair in two ways: 1) by plotting the distribution of changes in ROI orientations between session and comparing it to chance, calculated by shuffling neuron identity between session 1000 times, and 2) plotting ROIs of all neurons between two sessions and looking for systematic shifts in neuron ROIs that could lead to false negatives/positives in the registration." All session-pairs (except those few in which we could not synchronized imaging and behavioral data as noted above) met the above two criteria and were thus included in our analysis.

Cells that had calcium activity in the first session (NEUTRAL) arena for which we did not identify a matching neuron in the second session (SHOCK) were classified as OFF cells. Likewise, neurons active in the SHOCK arena with no matching partner in the NEUTRAL arena were classified as ON cells.

All neuron registrations were cross validated by overlaying ROIs from each session and evaluating their match by eye. In a few cases, we noticed erroneous registrations and adjusted our between-session neuron alignment by calculating the rigid geometric transformation using 4-5 cell ROIs active in both sessions.

Neural Discrimination Metrics

The extent to which gross hippocampal ensemble activity differed between arenas was calculated in two ways. First, we calculated the proportion of cells that turned ON and OFF between arenas divided by the total number of cells active in either arena.

Next, we calculated the extent to which each neuron active in both arenas distinguished between arenas by changing its event rate in a manner analogous to $DI_{Fr.}$ However, we took the absolute value to account for the fact that both positive and negative event rate changes could reflect neural differentiation between arenas. Then, we took the mean across all neurons to obtain a neural discrimination index (DI_{Neuron}):

$$DI_{Neuron} = \left| \frac{ER_{Neutral} - ER_{Shock}}{ERz_{Neutral} + ER_{Shock}} \right|$$

Placefield Analysis

Calcium transients occurring when the mouse was running greater than or equal to 1.5cm/second were spatially binned (1cm by 1cm) and occupancy normalized following which place fields were identified and quantified in a manner similar to Kinsky et al. (2018), reproduced here:

"Spatial mutual information (SI) was computed from the following equations, adapted from (Olypher et al., 2003)

$$I_{pos}(x_i) = \sum_{k=0}^{1} P_{k|x_i} \, log \left(\frac{P_{k|x_i}}{P_k}\right)$$

$$SI = \sum_{i=1} P_{x_i} \, I_{pos}(x_i)$$

where:

- P_{xi} is the probability the mouse is in pixel x_i
- P_k is the probability of observing *k* calcium events (0 or 1)
- $P_{k|xi}$ is the conditional probability of observing *k* calcium events in pixel x_i.

The SI was then calculated 1000 times using shuffled calcium event timestamps, and a neuron was classified as a place cell if it 1) had at least 5 calcium transients during the session, and 2) the neuron's SI exceeded 95% of the shuffled SIs…We defined the extent of a place field as all connected occupancy bins whose smoothed event rate exceeded 50% of the peak event rate occupancy bin."

Since spatial mutual information is biased by the number of samples (Olypher et al., 2003), we re-sampled the behavioral tracking data to match that of the imaging data (20Hz). This required up-sampling the SHOCK arena data (3.75Hz->20Hz) and down sampling the NEUTRAL arena data (30Hz->20Hz).

Placefield similarity between sessions was assessed by first smoothing the 2-d occupancy normalized event rate maps with a gaussian kernel (2.5cm std), flattening the smoothed maps into a vector, and then performing a Spearman correlation between all neurons active in both sessions. To quantify chance-level place field similarity we randomly shuffled the mapping between neurons from the first to the second session before performing the Spearman correlation. We then repeated this procedure 100 times.

To assess the possibility that the configuration of place fields rotated together coherently between sessions (Kinsky et al., 2018), we again performed a Spearman correlation but after rotating the 2-d occupancy map in the second session 90 degrees. Since, due to small camera distortions, some 2-d occupancy maps were not square, one some occasions we resized (minimally) the second map to match the size/shape of the first map using the reshape function in Python's numpy package prior to correlate the two maps. We repeated this in successive 90 degree increments and then took the mean correlation of all neurons that were active in both

sessions to determine the optimal/“best” rotation of the place field map as that which maximized the correlation between sessions.

We also performed a “center-out” rotation analysis to assess coherent place field rotations between sessions. First, the angle to the pixel with the maximum occupancy normalized event rate was identified for each cell. Second, this angle was recalculated for the same cell in a different session in the same box. These two angles were subtracted to get the “center-out” rotation between sessions. Sessions which exhibited a coherent rotation displayed a peak in a histogram of center-out angles at 0, 90, 180, or 270 degrees, while sessions which exhibited global remapping exhibited a uniform distribution of rotation angles.

Freeze-tuned Cell Analysis

Freeze onset and offset times were first identified for each mouse/session as noted in the *Behavioral Tracking and Fear Metrics* section above. We then formed calcium event rasters using the neural activity for each cell +/- 2 seconds from freeze onset, organizing the data into a *nfreeze_onsets x ntime_bins* array. We then summed this raster along the 0th dimension to get a freeze tuning curve. To calculated significance, we randomly, circularly shifted the putative spiking activity for a cell and calculated a shuffled tuning curve in a similar manner to the actual data. We repeated this procedure 1000 times, and calculated significance for each time bin as the number of shuffles where the shuffled tuning exceeded the actual tuning curve divided by 1000. Last, we designated cells as significantly freeze-tuned if they had 3 or more bins with $p < 0.01$ and were active on at least 25% of freezing events.

Covariance Analysis

Putative spiking activity for each cell was first binned into 0.5 second windows and z-scored after binning, forming a *ncells x nbins* array. The covariance of this array was then calculated using the *cov* function in numpy. For between-session comparisons, cells active in both sessions were matched up and a new array was formed with the base (1st) session covariance in the lower diagonal and the registered (2nd) session in the upper diagonal. All entries along the main diagonal were ignored.

<u>Author Contributions</u>

Conceptualization: N.R.K with the help of Howard Eichenbaum; Methodolgy :N.R.K; Software: N.R.K., E.A.R; Validation: N.R.K; Formal Analysis: N.R.K, D.O.O., E.A.R; Investigtion: N.R.K., D.O.O., E.A.R.; Data Curation: N.R.K., D.O.O., E.A.R.; Writing – original draft preparation: N.R.K.; Writing – review and editing; N.R.K, D.O.O, E.A.R., K.D., S.R.; Visualization: N.R.K.; Project Administration; N.R.K, S.R.; Funding Acquisition: N.R.K., K.D., S.R.

<u>Competing Interests</u>

The authors declare no competing interests.

FIGURE LEGENDS

Figure 1: Neural discrimination between arenas predicts specificity of fear learning. A) Schematic of the behavioral paradigm. Mice freely explored two distinct arenas (neutral and shock) for 10 minutes each day. Mice underwent mild contextual fear conditioning on day 0 in the shock arena followed by immediate I.P. administration of anisomycin or vehicle in their home cage. Memory recall test were conducted 4 hours post-shock and 1, 2, and 7 days post-shock. The time of each session is referenced to the shock session. **B)** (left) Learner (Control) mice freezing on all days. Red = shock arena, Blue = neutral arena. *p=1.3e-0.5 shock – neutral freezing from days -2/-1 to days 1/2 one-sided t-test (n=4 mice). (right) Same but for Non-Learner (Control) mice (n=3 mice). **C)** (left) Neural overlap plots between Neutral and Shock arenas for an example Learner mouse on day -1, before shock. Green = cells active in the Shock arena only, yellow = cells active in the Neutral arena only, orange = cells active in both arenas. (right) Same for example Non-Learner on day -2 showing higher overlap of active cells between arenas. **D)** Same as B but for ANI group **E)** Mean neural discrimination between arenas (same day, days -2 to -1 and 1 to 2) vs. within arenas (same arena, days -2 and -1, days 1 and 2). *p=2.35e-8 (ρ=-0.56) Spearman correlation**.** **F)** Example calcium activity from the Learner mouse shown in C (left) for cells active in both arenas. Black = calcium trace, Red = putative spiking activity during transient rises. Top row shows Shock arena preferring cells, bottom row shows Neutral arena preferring cells. **G)** Behavioral discrimination between arenas after shock (Days 1-2) shows formation of a specific fear memory for Learners only, by definition (positive = more freezing in neutral arena, negative = more freezing in shock arena, 0 = equal freezing in both arenas). *p=0.022, **p=0.00038 1-sided t-test **H)** Neural discrimination between arenas BEFORE shock indicates Learners formed more distinct representations of each arena prior to learning. Same conventions as F. *p=0.030, +p=0.059 two-sided t-test. **I)** Neural overlap between arenas correlates with specificity of fear memory on days 1-2 for Learners but not Non-Learners. +p=0.059 (ρ=-0.56) for Learners. **J)** Same as I) but plotting behavioral discrimination vs. overlap ratio between arenas on Days 1-2. *p=0.033 (ρ=0.61).

Figure 2: Anisomycin accelerates cell turnover and stifles learning-related place field remapping **A)** Cell overlap ratio with Day -2 session, Control mice. Blue = within shock arena, red = shock v. neutral arena **B)** Same as A) but for anisomycin mice **C)** Change in overlap ratios from a and b. *p=0.028, **p=0.00024 two-sided t-test **D)** Number of active neurons observed each day, normalized to day -1. *p=0.039 two-sided t-test **E)** Stable place field. (*top)* Example mouse trajectory (black) with calcium activity (red) overlaid for the same cell from day -2 to -1 in shock arena, *(bottom)* occupancy normalized rate maps for the same cells **F)** Same as E) but for a different cell that remaps from day -2 to day 1 in the shock arena. **G)** Place field correlations for all mice before shock (Days -2 and -1). *p<0.0032 Learners vs ANI and Non-Learners vs ANI, **p=1.9e-6 Non-Learners vs ANI, k-s test after Bonferroni correction. **H)** Same as G) but for days after shock. *p=0.045 Learners vs Non-Learners and p=0.0059 Non-Learners vs ANI, +p=0.1 Learners vs ANI **I)** Same as G) but to assess learning-related remapping from before to after shock. *p=0.00021 Learners vs Non-Learners and p=3.4e-11 Non-Learners vs ANI, +p=0.12 Learners vs ANI **J)** Place field correlations before shock broken down by mouse **K)** Same as J) but for sessions after shock **L)** Same as J) but from before to after shock. p=0.002 mixed ANOVA, group x arena interaction. *p=0.025 Non-Learners vs ANI, **p=0.013 Learners vs Non-Learners, ***p=0.034 Learners vs ANI, post-hoc pairwise t-test after Bonferroni correction.

Figure 3: ANI administration suppresses the development of coordinated freeze-related neural activity. **A) and B)** Example traces from two freeze-cells which exhibit coordinated activity prior to freezing event during the Day 1 memory recall session in the shock arena, red = putative spiking activity. Pink = cell shown in C, blue = cell shown in E. **C)** Proportion of freeze-tuned cells detected each day across all groups. Green = freezing epochs. **D) and E)** Example Learner freeze-tuned cells identified on shock day 1 (bold) tracked across sessions. Peri-event calcium activity rasters are centered on freeze onset time (solid green). Dashed green = baseline calcium event probability, red solid = peri-freeze calcium event probability, bins with p<0.01 (circular permutation test) noted with red bars at top. D/E

corresponds to pink/blue cells shown in A-B. **F)** Same as D and E but for ANI mouse shock cell identified during the 4 hour session. **G)** Change in peak peri-freeze calcium event probability for all freeze-tuned cells detected during the 4 hour session. **H)** Same as G but for freeze-tuned cells detected during Day 1 recall session. $p < 0.02$ 1-way ANOVA each day separately, *p=0.02, **p=0.001, ***p=0.0006 post-hoc Tukey test. **I)** Freeze-tuned cells exhibit increased covariance in the Control compared to the ANI group. Mean covariance of freeze-tuned cells from each session shown. p=0.016 two-way ANOVA (Time). *p=0.018 post-hoc pairwise t-test (two-sided) after Bonferroni correction. **J)** Small but significant increase in covariance of all cells for Control mice during the 1 day recall session. p=0.0015 (Time), 0.005 (Group), 0.036 (Group x Time) two-way ANOVA. *p=0.014, **p=0.008, ***p=0.004 post-hoc pairwise t-test (two-sided) after Bonferroni correction. **K)** Mean covariance of freeze-tuned cells detected during the 4 hour session tracked across sessions. P=0.005 (Group), 0.04 (Group x Time) two-way ANOVA. p=0.014, +p=0.09 post-hoc pairwise t-test (two-sided) after Bonferroni correction. **L)** Same as K but for freeze-tuned cells detected during Day 1 recall session. p=0.0003 (Group) two-way ANOVA. *p=0.016 post-hoc pairwise t-test (two-sided) after Bonferroni correction.

Figure S1: **Behavioral Paradigm and Neuronal Recordings**

A) Control mice freezing on all days. Red = Shock arena, Blue = Neutral Arena *p=0.025 shock – neutral freezing from days -2/-1 to days 1/2, one-sided t-test (n=7 mice). **B)** Distribution of DI_{beh} scores for all Control mice on days 1-2. Dashed line indicates cutoff between Learners and Non-Learners. **C)** Cell overlap 1 day apart in the same arena (days -2 to -1 and 1 to 2) vs. cell overlap between arenas on the same day (days -2, -1, 1, 2) for all Control mice. *p=1.7e-5, r=0.74 Spearman correlation.

Figure S2: Non-specific effects of Anisomycin include a reduction in locomotion

A) 4 mice were given I.P injections of anisomycin only (no shock) and their locomotion was tracked over 24 hours. Normal activity did not return to baseline until between 6 and 24 hours later.

Figure S3: **Coherent Place Field Rotations Observed Between Sessions**

A) Example animal trajectories from Neutral arena Day -2 (top row) and Day -1 (middle row) with calcium activity overlaid (red). Each column corresponds to one cell. Bottom row shows data rotated 90 degrees, demonstrating a coherent rotation of spatial activity for all neurons. **B)** Smoothed, occupancy normalized calcium event maps corresponding to data shown in A). **C)** The angle from the center of the arena to each cell's maximum intensity place field center was calculated for each session (center-out angle). The distribution of center-out angles plotted, demonstrating a coherent rotation of place fields from Day -2 to Day -1 by 90 degrees. **D)** Place field correlations (smoothed event maps) between sessions indicate apparently low stability across days without considering rotations, giving the false impression that the place field map randomly reorganizes between sessions. **E)** High correlations were observed after considering a coherent 90 degree rotation between sessions, indicating that place fields retain the same relative structure but rotate together as a whole. **F)** Mean correlations for each mouse and **G)** combined correlations for all neurons calculated without considering rotations gives the impression of instability Before/After shock and heightened remapping for all groups from Before to After learning.

Figure S4: Place field correlations with STM (4 hour) session

A) Distribution of place field correlations for all mice combined for Before (Day -2 and Day -1) vs STM (4hr) sessions. **B)** Same as A) but for STM vs After (Days 1-2) sessions. *p=0.0217 Non-Learners v ANI in Shock arena, **p=0.00014 Non-Learners v ANI Neutral arena, ***p=3.6e-8 Learners v Non-Learners Neutral Arena. All p-values after Bonferroni correction for 3 comparisons. **C)** Before v STM mean place

field correlations for each mouse/session-pair. **D)** Same as C but for STM v After **E)** Mean height of calcium transient peaks for all cells matched from day -1 to 4 hour session. p>0.63 both groups, two-sided t-test. **F)** Same as E) but tracking cells from day -1 to day 1, p>0.68 both groups.

Figure S5: Population Vector (PV) correlations indicate that anisomycin disrupts cell turnover

A)-E) 1D PV correlations between sessions including only cells active in BOTH sessions. **A)** Before (Days -2 and -1), *p=0.006 Shock v Neutral arena, mixed ANOVA **B)** After (Days 1 and 2) *p=0.024 Shock v Neutral Arena, mixed ANOVA **C)** Before v After, p < 0.003 Neutral v Shock arena and Group x Arena interaction, mixed ANOVA. *p<0.001, +p=0.056 t-test (two-sided) after Bonferroni correction **D)** Before v STM (4 hour), p=0.052 Group x Arena interaction, mixed ANOVA **E)** STM v After *p=0.004 Neutral v Shock arena, mixed ANOVA. **F)-J)** 1D PV correlations including cells active in EITHER session (includes new and silent cells). **F)** Before *p<0.001 Shock v Neutral arena, mixed ANOVA **G)** After, p > 0.12 all comparisons mixed ANOVA **H)** Before v After, p<0.003 all comparisons mixed ANOVA *p=0.023 Learners v ANI, **p=0.007 Non-Learners v ANI, +p=0.083 Non-Learners v ANI t-test (two-sided) after Bonferroni correction **I)** Before v STM p<0.005 Arena and Group comparisons, p=0.059 Arena x Group interaction, *p=0.004 Learners v ANI, **p=0.033 Learners v ANI t-test (two-sided) after Bonferroni correction **J)** STM v After p<0.022 Arena and Group comparisons, p=0.103 Arena x Group interaction, *p=0.041 Learners v ANI, **p=0.003 Non-Learners v ANI, ***p=0.003 Non-Learners v ANI t-test (two-sided) after Bonferroni correction**.** Green = Learners, Orange = Non-Learners, Blue = ANI.

Figure S6: ANI administration impacts on freeze-tuned cells are not a result of a general disruption of neuronal coactivity

A)-C) Example freeze-tuned cells tracked across sessions forward and backward in time from the day indicated in bold. Peri-event calcium activity rasters are centered on freeze onset time (solid green). Dashed green = baseline calcium event probability, red solid = peri-freeze calcium event probability, bins with p<0.01 (circular permutation test) noted with red bars at top. D/E corresponds to pink/blue cells shown in A-B. **A)** Example cell from Non-Learner **B)-C)** Example cells from two different Learners. **D)** Proportion freeze-tuned cells detected in neutral arena across days **E)** Mean covariance of all cells in Neutral arena prior to learning exhibit small changes, compare y-axis to Figure 3J. p=0.012 two -way ANOVA, *p=0.04 post-hoc pairwise two-sided t-test after Bonferroni correction. **F)** Mean covariance freeze-tuned cells after randomly downsampling the number of freeze events to match the average number observed during days -2 and -1. p=0.02 two-way ANOVA, +p= 0.055 post-hoc pairwise two-sided t-test after Bonferroni correction, mean of 100 downsampling iterations. **G)** Same as F) but for all cells p0.0015 two-way ANOVA, *p=0.02, **p=0.008, ***p=0.004 post-hoc pairwise two-sided t-test after Bonferroni correction. **H)** Mean covariance of freeze cells excluding peri-freeze times (freeze start +/- 2 sec) from neural activity. P=0.012 (Time) two-way ANOVA. **I)** Same as H) but for all cells. p=0.001 (Time) two-way ANOVA *p=0.045, **p=0.006, ***p=0.004 post-hoc pairwise t-test (two-sided) **J)** Mean covariance of freeze cells before, 4 hours after, and 1-2 days after learning/ANI injection broken down by learning group. p=0.014 (Time) two-way ANOVA. *p=0.04 post-hoc pairwise t-test (two-sided) **K)** Same as J) but for all cells. p=0.0008 (Time) two-way ANOVA. *p=0.012, **p=0.0028 post-hoc pairwise t-test (two-sided) **L)** Same as J) but tracking freeze-tuned cells from the 4 hour session forward/backward in time. p=0.006 (Time) two-way ANOVA. +p=0.13 post-hoc pairwise t-test. **M)** Same as L) but for 1 day freeze cells tracked forward/backward in time.

Figure S7: Anisomycin does not globally disrupt electrophysiological signal in hippocampal neurons. Neural activity was tracked across ~5 hours before and after systemic administration of anisomycin. **A)** Cross correlograms for all single and multi-unit activity combined are shown from the pre epoch in a rest box (15 minutes), running on a novel track immediately following anisomycin injection (45

882 minutes), post epoch in the rest box (3.5 hours), running on a second novel track (45 minutes), and a
883 second post epoch in the rest box (15 minutes). Clear modulation of firing at the theta timescale is
884 observed. **B)** Example trace from electrode in pyramidal cell layer of CA1 showing theta activity 10
885 minutes and 4 hours 15 minutes post injection anisomycin injection. **C)** Example sharp wave ripple events
886 occurring from 25 minutes to hours 15 minutes post anisomycin injection.